Journal of Digital Imaging

A Motion Compounding Technique for Speckle Reduction in Ultrasound Images

Cheng-Hsien Lin,[1] Yung-Nien Sun,[1] and Chii-Jeng Lin[2]

The quality of ultrasound images is usually influenced by speckle noise and the temporal decorrelation of the speckle patterns. To reduce the speckle noise, compounding techniques have been widely applied. Partially correlated images scanned on the same subject cross-section are combined to generate a compound image with improved image quality. However, the compounding technique might introduce image blurring if the transducer or the target moves too fast. This blurring effect becomes especially critical when assessing tissue deformation in clinical motion examinations. In this paper, an ultrasound motion compounding system is proposed to improve the quality of ultrasound motion sequences. The proposed motion compounding technique uses a hierarchical adaptive feature weighted motion estimation method to realign the frames before compounding. Each frame is first registered and warped to the reference frame before being compounded to reduce the speckle noise. Experimental results showed that the motion could be assessed accurately and better visualization could be achieved for the compound images, with improved signal-to-noise and contrast-to-noise ratios.

KEY WORDS: Ultrasound compounding, speckle reduction, motion estimation, soft tissue motion

INTRODUCTION

Ultrasound imaging is a real-time imaging technique. It has been an important tool in clinical investigations for many years. However, the quality of ultrasound images is usually degraded by coherent wave interference, known as speckle, which shows up as small scale brightness fluctuations or mottling superimposed on all parts of the image, especially in homogeneous tissue regions.[1,2] Furthermore, speckle patterns can also be temporally decorrelated by out-of-plane motion or by the non-uniform movement of sub-resolution scatters. Hence, speckle artifacts significantly impact imaging performance by reducing contrast resolution and obscuring small structures.

To reduce speckle noise, ultrasound compounding techniques have been widely investigated.[3–5] Ultrasound compounding aims to improve image quality by averaging several coplanar ultrasound frames into a single image. Conventionally, decorrelation between measurements can be introduced by imaging using different spatial positions,[6–8] frequency ranges,[9] or strain conditions.[10] In principle, compound imaging starts by scanning frames of the target in the same imaging plane but from different viewing angles (frequencies or strain conditions), which produce different artifact patterns. Averaging these independent frames suppresses the artifacts and reinforces the real structures. Hence, the primary assumption of compounding is that by averaging partially correlated measurements, speckle brightness variations can be reduced without affecting the original image contrast.

In other words, the ultrasound compounding mechanism integrates the aligned information from

[1]From the Department of Computer Science and Information Engineering, National Cheng Kung University, No. 1, Ta-Hsueh Road, Tainan, Taiwan, Republic of China.

[2]From the Department of Orthopaedics, National Cheng Kung University Hospital, National Cheng Kung University, Tainan, Taiwan, Republic of China.

Correspondence to: Yung-Nien Sun, Department of Computer Science and Information Engineering, National Cheng Kung University, No. 1, Ta-Hsueh Road, Tainan, Taiwan, Republic of China; tel: +886-6-2757575; fax: +886-2-747076; e-mail: ynsun@mail.ncku.edu.tw

Online publication 7 January 2009

doi: 10.1007/s10278-008-9172-6

ultrasound signals to improve the ultrasound image quality. This type of function is usually performed with an ultrasound system specially designed for compounding and is completed online at the imaging stage. Previous tests with both experimental and commercial spatial compounding systems have shown that ultrasound compounding can improve some aspects of the appearance of breast anomalies, carotid plaques, and so forth.[11–14] Compound imaging provides various benefits, such as a reduction in image clutter and an improvement in the delineation of target objects. Usually, this compounding technique is applied to static target imaging and can suffer from blurring due to misalignment between frames if the transducer or the target moves too rapidly.[15–17] This blurring effect causes a significant reduction in the sharpness of compound images, especially in ultrasound motion sequences. Generally, the more frames used for compounding, the greater the improvement in image quality and the greater potential for motion blurring. This results in a tradeoff between improving image quality and minimizing motion blurring.

In contrast with the existing compounding methods, we designed a new software-based ultrasound compounding system that improves the quality of ultrasound images with moving targets. In our setup, the temporal image sequences acquired from a regular ultrasound system can be further processed for compounding, which cannot normally be done without a compound imaging system. One major advantage of the proposed method is the effectiveness and efficiency of nonrigid registration, which does not require any special hardware platform or acoustic probe. Thus, the method can be implemented as standalone image compounding software or as part of an ultrasound compounding hardware system.

In the proposed system, we designed an adaptive feature weighted mechanism with a hierarchical structure to estimate the dense motion field from the ultrasound image sequence. Adjacent frames are first registered and warped to match the reference frame and then averaged to generate the compound image. In experiments, the speckle reduction and contrast improvement performances were tested based on several criteria. The compounding results for both phantom and in vivo clinical images showed significant improvement in both quantitative and visual appearance.

METHODS

Generally, difficulties in accurately estimating the motion field in ultrasound images arise from speckle noises and speckle decorrelation. Several matching criteria in block-matching algorithm have been tested to recover the tissue motion from ultrasound images.[18] On the other hand, due to the local homogeneity of motion, the smoothness constraint that tissue motion is continuous is usually adopted.[19,20] In the following sections, we will briefly introduce the hierarchical feature weighting algorithm[21] which is used to estimate the motion fields in the proposed motion compounding technique.

Let $\boldsymbol{a}_i$ and $\boldsymbol{b}_i$ represent the vectors for all intensities of the processing and the reference matching blocks displaced by the corresponding motion vector $\boldsymbol{v}_i=(u_i, v_i)$, respectively. The optimal estimate of $\boldsymbol{v}_i$, $\hat{v}$, is obtained by maximizing for each i of the following conditional probability density function:

$$\hat{v} = \arg\max_{v_i} p(\boldsymbol{a}_i|\boldsymbol{b}_i, v_i). \tag{1}$$

Assuming $\boldsymbol{a}_i=\mathbf{b}_i+\mathbf{n}_i$ and $p_n(n)$ is the probability density function of each element of the vector $\boldsymbol{n}_i$, the maximization of Eq. 1 is equivalent to the maximization of Eq. 2 [22]:

$$\hat{v} = \arg\max_{v_i} \prod_{j=1}^{k} p_n\left(a_{ij} - b_{ij}\right), \tag{2}$$

where i is the index of corresponding positions in the search window, and j is the index of pixels in the matching block with size k. If n is a generalized zero-mean Gaussian noise, the maximization of Eq. 2 is equivalent to the minimization of the following objective function:

$$\hat{v} = \arg\min_{v_i} \sum_{j=1}^{k} \left|a_{ij} - b_{ij}\right|^c. \tag{3}$$

That is, the estimated solution is defined as the relative displacement of the block with the minimal value of this objective function in a block-matching-based algorithm. The most commonly used objective functions is the sum of absolute difference which is corresponding to $c=1$, because of its simplicity and fast computation time.

To maintain both accuracy and efficiency, Bayesian estimation is used for incorporating the a priori knowledge to restrict the space of possible solutions. By using the maximum a posteriori estimator,[23] the optimal estimate $\hat{v}$ can be obtained by maximizing the following a posteriori likelihood probability distribution:

$$\hat{v} = \arg\max_{v_i} P(v_i|a_i,b_i) = \arg\max_{v_i} \frac{P(a_i|b_i,v_i)P(v_i|b_i)}{P(a_i|b_i)} \propto \arg\max_{v_i} P(a_i|b_i,v_i)P(v_i|b_i), \tag{4}$$

where $P(\mathbf{a}_i|\mathbf{b}_i)$ is independent of the estimated parameters and can be omitted. That is, restriction of possible solutions is made, based on the a priori information, $P(v_i|\mathbf{b}_i)$, to make the motion estimation problem well-posed such that a stable and unique solution can be found.

To reduce the computational complexity of the full search block-matching algorithm, several fast algorithms have been proposed.[24–26] Here, a hierarchical method is adopted in the system. First, for each image, an image pyramid can be defined as a sequence of image levels $\{L^0,L^1,\ldots,L^{k-1},L^k\}$, where the resolution superscript will span from 0 for the finest resolution to k for the coarsest one. This reduction process can be formed by successively averaging over 2×2 neighboring pixels on the lower levels. The block-matching algorithm can then be performed on the corresponding image pyramids based on a top-down strategy, as illustrated in Figure 1. In the following experiments, three more image levels (k=3) are generated to build the pyramid.

Using this hierarchical structure, maximizing the a posteriori likelihood probability defined in Eq. 4 can be rewritten as:

$$\hat{v}_l = \arg\max_{v_i^l} P\left(v_i^l|a_i^l,b_i^l\right) \propto \arg\max_{v_i^l} P\left(a_i^l|b_i^l,v_i^l\right)P\left(v_i^l|b_i^l\right), \tag{5}$$

where l is the level index of the image pyramid. To define possible search candidates inherited from the hierarchical structure, an a priori distribution of motion vectors given b_i^l can be defined as:

$$P\left(v_i^l|b_i^l\right) = \begin{cases} 1, & \text{if } v_i^l \in N\left(v_{i'}^{l+1}\uparrow_2\right) \\ 0, & \text{otherwise} \end{cases}, \tag{6}$$

where i' is the corresponding position of i in the coarser level, $v_{i'}^{l+1}\uparrow_2$ is the corresponding motion vector projected (up-sampled) from the coarser level of the pyramid, and $N(v)$ is the neighboring motion estimates around v. Thus, the a priori distribution constrains the candidate motion field space with respect to the projected motion vector,

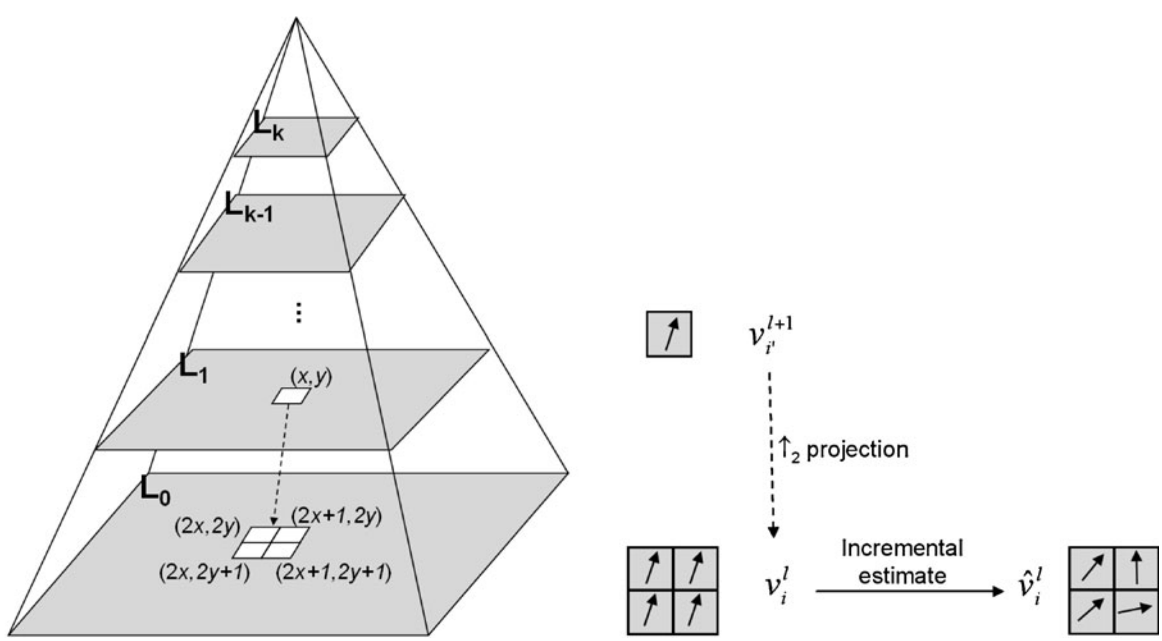

Fig. 1. Illustration of the hierarchical motion estimation.

and the a posteriori probability can be only evaluated in the defined small search space. In practical, a 3×3 search range is enough. That is, a maximum search length one is enough because a search length two implies a search length one which has already been evaluated in the upper level. Note that, in the coarsest level, this prior information is not considered. Generally, duplication or a linear interpolation approximation is used for projecting the motion field in the traditional methods. However, homogeneous regions of constant intensity give little motion information and pixels may be unreliable in determining their correspondences for reasons besides noise. To cope with these problems, we adopt a new adaptive feature weighted filtering method[21] to improve the estimation accuracy of the hierarchical MAP estimator.

Usually, motion vectors associated with the same object should be similar, resulting in motion smoothness between neighboring pixels. Therefore, the projected motion vector can be more robustly estimated by the following weighting operator:

$$v^{l}_{i=(x,y)} = \sum_{i'\in Q(x/2,y/2)} w^{l+1}_{i'} \times v^{l+1}_{i'}, \qquad (7)$$

where image block Q is the filtering mask centered at image position $(x/2,y/2)$ in pyramid level $l+1$, and $v^{l+1}_{i'}$ represents the corresponding motion vectors. The weighting factors $w^{l+1}_{i'}$ are normalized such that the sum of weights is equal to one which implies the convex combination. Thus, the resultant motion vector can be obtained as a weighted mean vector which is within the convex hull of given vectors. In this paper, motion estimation is based on the assumptions that the motion field varies smoothly within the tissue region and that the motion estimates at feature pixels are much more reliable. This weighting process can be illustrated in Figure 2.

For this feature-based technique, feature identification is naturally the most important task and

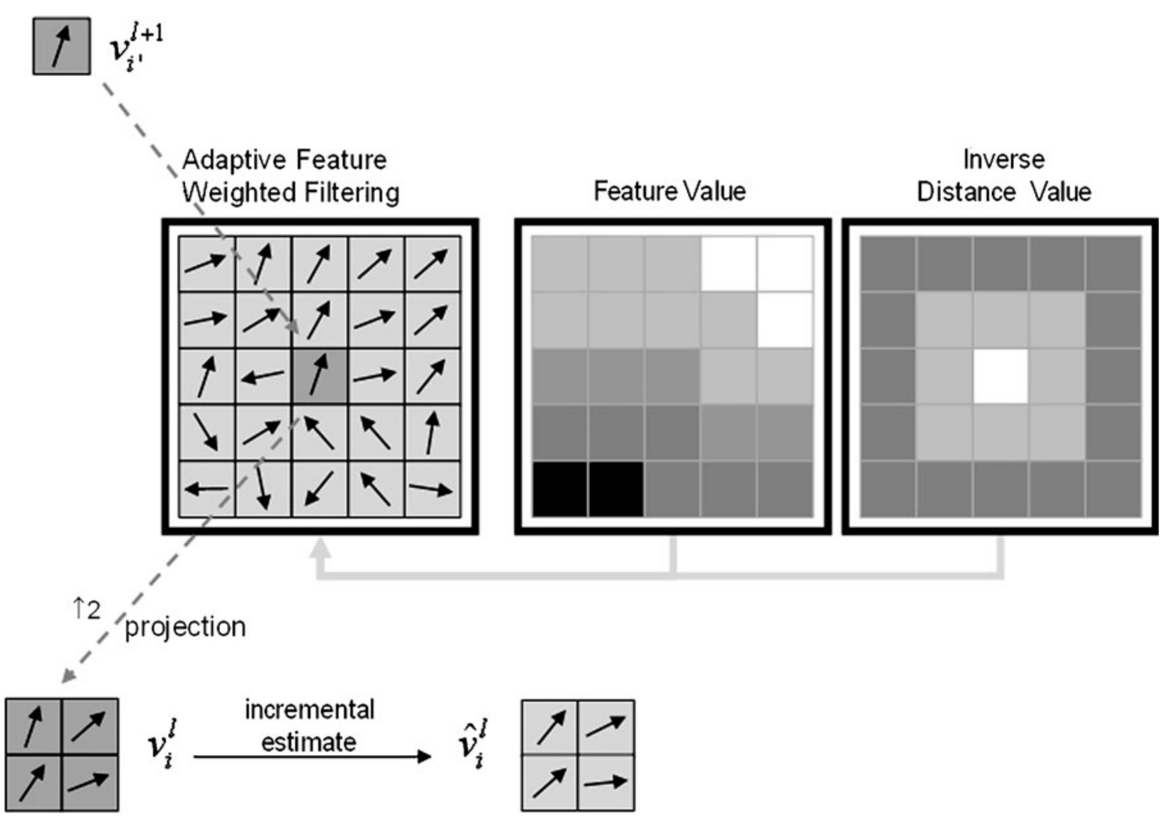

Fig. 2. Illustration of the adaptive feature weighted filtering method.

detection based on speckle statistics is the most reliable way for identifying features. It has been shown that the local mean of speckle noise in ultrasound B-mode images is proportional to the corresponding local variance.[27–29] A local statistics, α_i, representing the ratio of local variance, σ_i^2, to local mean, μ_i, at image location i, can hence be calculated as the characteristic value:

$$\alpha_i = \frac{\sigma_i^2}{\mu_i}. \tag{8}$$

The local statistics α can be easily measured on the image and a smaller α indicates a higher possibility that the processing pixel belongs to a homogeneous region. Hence, α can be regarded as the feature values and motion estimation with these temporally stable features should be more accurate and reliable.

In addition, an inversely distance-weighted constraint in is adopted to preserve the smoothness property. Based on the assumption that the tissue motion field is continuous, the motion vector being estimated is strongly influenced by the motion vectors on the nearby tissues, but is less influenced by those of the tissues further away. Therefore, the weighting factor in Eq. 7, $w_{i'}^{l+1}$, is designed to include both the local statistics, α, and the inverse distance factor. This weighting process is performed on a fixed running window with the weights adaptively adjusted according to the local statistics. The weighting factor can be defined as:

$$w_{i'}^{l+1} = g_1 \times \frac{1/\left(\left(d_{i'}^{l+1}\right)^a + b\right)}{\sum_{i'' \in Q} 1/\left(\left(d_{i''}^{l+1}\right)^a + b\right)} + g_2 \times \frac{\alpha_{i'}^{l+1}}{\sum_{i'' \in Q} \alpha_{i''}^{l+1}}, \tag{9}$$

where g_1 and g_2 are scalar parameters, Q is the filtering mask, d is the distance from the image pixel to the center of the filtering mask, and α is the local variance-to-mean ratio. In the following experiments, the value of g_1 and g_2 are both empirically selected as 0.5.

In Eq. 9, the first term is an inversely distance-weighted parameter. In the experiments described below, the selected value of a is 2, which means the smoothness term is inversely square distance weighted. The parameter b is given a small value to avoid the problem caused by a zero distance. The second term is a feature weighted value dependent on the local variance-to-mean ratio of the image pixel. When the value is large, the corresponding pixel very likely belongs to some stable patterns and is thus highly weighted. Generally, pixels far from the center are less related to the processing pixel and can be omitted because the corresponding weighting values are small according to the inversely distance-weighted strategy. In practical, an 11×11 filtering mask is large enough and performs well in the following experiments.

In the proposed motion compounding technique, as illustrated in Figure 3, the original image is referred to as the reference image. Then, a motion-compensated technique which is usually used in video coding,[30] is adopted to register and warp the adjacent frames of reference image with the estimated motion fields. As mentioned previously, frame averaging can induce image blurring if the transducer or the target moves too rapidly. With the estimated motion fields, each frame is hence spatially matched and tissue motion-corrected to the reference frame before being added to the compound image. The compound image can then be created by some compounding strategies with the recorded warped images.

Usually, this compounding task is solved by frame averaging and the estimate of the original signal $\hat{X}$ based on N observations, X_1, X_2,..., X_N, can be given by averaging the warped speckle images over all frames:

$$\hat{X} = \frac{1}{N} \sum_{i=1}^{N} X_i \tag{10}$$

Generally, the more frames used for compounding, the greater the improvement in image quality. In the following experiments, nine frames are compounded to generate a single compound image, that is, N=9.

To test performance of different compounding strategies, several techniques such as mean, median, and scaled L_2 mean have also been investigated.[17,31,32] In general, according to these researches, there are no significant differences between the resultant images using different compounding strategies. In the system described, the compounding operator is replaceable and a mean operator is adopted for frame compounding. Generally, the

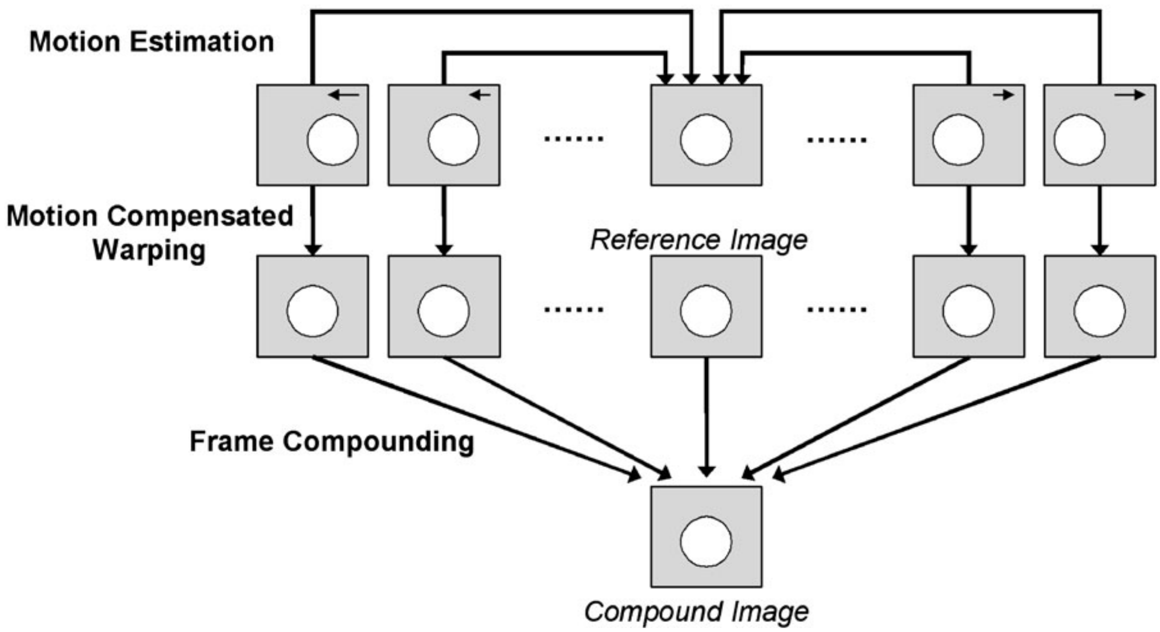

Fig. 3. Illustration of the motion compounding method.

intensity of a tracking material will not be consistent because of speckle decorrelations. The intensity will be degraded after applying the mean operator and the compound image will hence be a little darker than the original speckle image. To compensate for this intensity-degrading effect, the resulting compound image is normalized by multiplying a scale value, λ:

$$\lambda = \frac{\mu_{\mathrm{org}}}{\mu_{\mathrm{cmd}}}, \tag{11}$$

where μ_{org} and μ_{cmd} are the mean intensities of the original speckle image and the compound image, respectively. Thus, the mean intensity of the compound image is consistent with the mean intensity of the original speckle image. Note that, the intensity value is assigned with 255 when the normalized value is larger than 255.

EXPERIMENTAL RESULTS

Phantom Data Analysis

To show the motion compounding performance, the system was applied to both phantom and in vivo image sequences. First, in the phantom experiment, an image sequence was acquired with free-hand type compression using an increasing downward force applied by the probe. Figure 4a shows an example frame of this sequence. The B-scans of the phantom cross-section contain two regions with almost homogeneous statistical features: inside the circular region and the outside background. Figure 4b shows the estimated motion field using the proposed motion estimation method. The estimated motion field shows the overall longitudinal compression and a small lateral shift, which agreed with visual inspection. The compound image of Figure 4a is shown in Figure 4c.

To investigate the effect of motion compounding on image statistics, two regions were manually defined. Region 1 was completely inside the circle and region 2 was on the outside, as shown in Figure 4d. Assuming that each region had a uniform composition, all of the variance within a given region was mainly due to speckle noise and the amount of speckle noise present in each region could be objectively quantified by the signal-to-noise ratio (SNR). Specifically, the speckle SNR was calculated as the mean intensity, μ, divided by the standard deviation of intensity, σ, within the region. A high SNR corresponded to a low degree of speckle noise and thereby a smooth appearance. Another useful measure is the contrast-to-noise ratio (CNR), which is related to how easily different materials can be distinguished. The

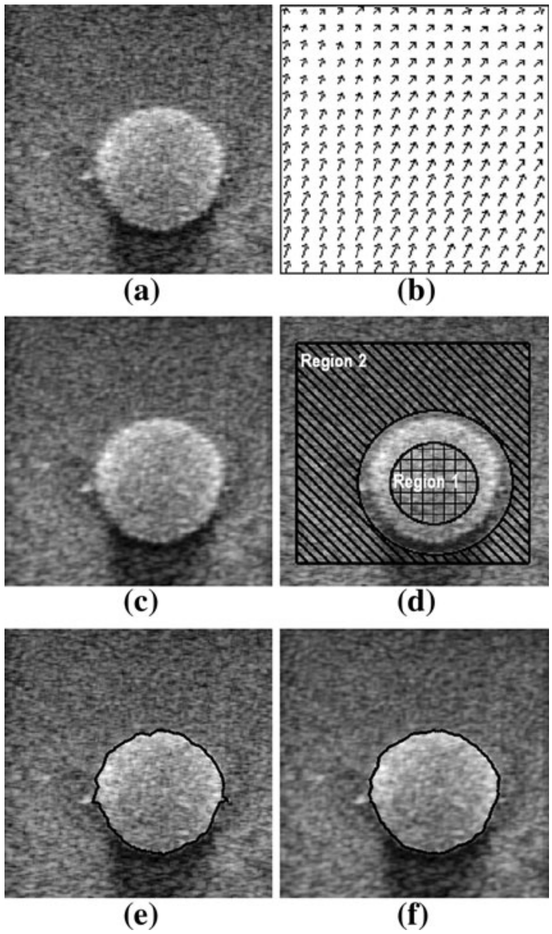

Fig. 4. Example frames of the phantom experiment: a the original speckle image, b the estimated motion field, c the compound image, d region definition of the phantom image, e and f the extracted boundaries of (a) and (c) by using the GVF snake, respectively.

speckle CNR was defined by $(\mu_o - \mu_b)/\sigma_b$, where μ_o and μ_b were the mean intensities within the object and background, respectively, and σ_b was the standard deviation of intensity within the background. In this phantom experiment, the SNRs of region 1 (object) and region 2 (background) before motion compounding were 5.89 and 4.54, respectively. After motion compounding, the SNRs of region 1 and region 2 had increased to 7.00 and 5.38, respectively. The CNRs before and after motion compounding were 1.52 and 1.79, respectively. The proposed motion compounding technique increased both the SNR and CNR by around 18%.

Generally, common spatial filters can also improve the SNR, but these decrease the spatial resolution of the speckle images. Usually, object segmentation is important in clinical use and segmentation accuracy can hence be adopted to evaluate the improvement in image quality. In medical applications, the most commonly used segmentation algorithm is the active contour model (snake). However, snakes usually fail to extract an accurate object boundary, resulting in a rather irregular boundary because of speckle noise. Therefore, an appropriate method of image preprocessing, providing clear and accurate delineation of object margins, is important for boundary extraction. To show the advantages of motion compounding for margin definition, the gradient vector flow (GVF) snake[33] was adopted to show its ability to extract object boundaries with and without applying motion compounding.

Figure 4e,f shows the extracted boundaries of the original speckle image and the compound image, respectively, by using the GVF snake with the same parameters and initial contour. As shown in Figure 4e,f, the extracted object boundaries were substantially better defined in the compound image. To validate the segmentation results, the extracted object boundaries could normally be compared with the ground truth. However, in this case, the correct boundaries were unknown because the phantom was compressed and the shape of the object was hence deformed. Therefore, a substitute criterion, the local curvature, was calculated to evaluate the segmentation results because the extracted shape of the object was supposed to be smooth. If we let $p_1=(x_1, y_1)$, $p_2=(x_2, y_2)$, ..., $p_n=(x_n, y_n)$ be n snake points along the extracted contour, the local curvature of p_i can be defined as $\|\mathbf{d_i}-\mathbf{d_{i-1}}\|$, where $\boldsymbol{d}_i$ and $\mathbf{d}_{i-1}$ are the normalized vectors of $\mathbf{p_{i+1}}-\mathbf{p_i}$ and $\mathbf{p_i}-\mathbf{p_{i-1}}$, respectively. In this experiment, the average local curvature of the GVF snake without motion compounding was 0.19±0.25 and was improved to 0.16±0.19 with motion compounding. A smoother contour could be extracted and both the average local curvature and its standard deviation were decreased by applying the motion compounding before boundary detection.

Clinical Data Analysis

Motion analysis in ultrasound imaging is commonly used as a diagnostic tool for investigating tissue deformation and providing a mathematical description of tissue mechanics. However, a fast acquisition speed might lead to a decrease in the spatial resolution, with poor definition of anatomical structures and high levels of speckle noise. To demonstrate the usefulness of the proposed compounding algorithm for in vivo image sequences, we undertook several ultrasound examinations with tissue motion, including musculoskeletal and myocardial experiments. The proposed motion compounding method was also compared with the spatial Gaussian smooth filter and the adaptive weighted median filter (AWMF),[27] which uses the local statistics weighting of the median filter to remove the speckle and preserve the signal boundary. These two methods are widely used in smoothing the speckle noise in ultrasound images.

In the musculoskeletal experiment, images were obtained by scanning the forearm in longitudinal cross-section. The images were taken from the muscle portion of the flexor digitorum profundus when the subject's middle finger moved from extension to flexion. In the imaging process, the probe was held by an expert and placed as parallel to the moving direction of the observed muscle as possible. An example frame is shown in Figure 5a and the estimated motion field using the proposed motion estimation method is shown in Figure 5b. From the motion vectors, it is easy to differentiate among the muscle groups involved in finger contraction. The compound images with and without applying the motion compensation are shown in Figure 5c,d, respectively. As shown in Figure 5c,d, the proposed motion estimation method could correctly compensate for the motion between frames, while the compound image without motion compensation shows a large number of artifacts caused by the motion blurring effect. In addition, spatial filters were applied to show their ability to enhance the speckle images.

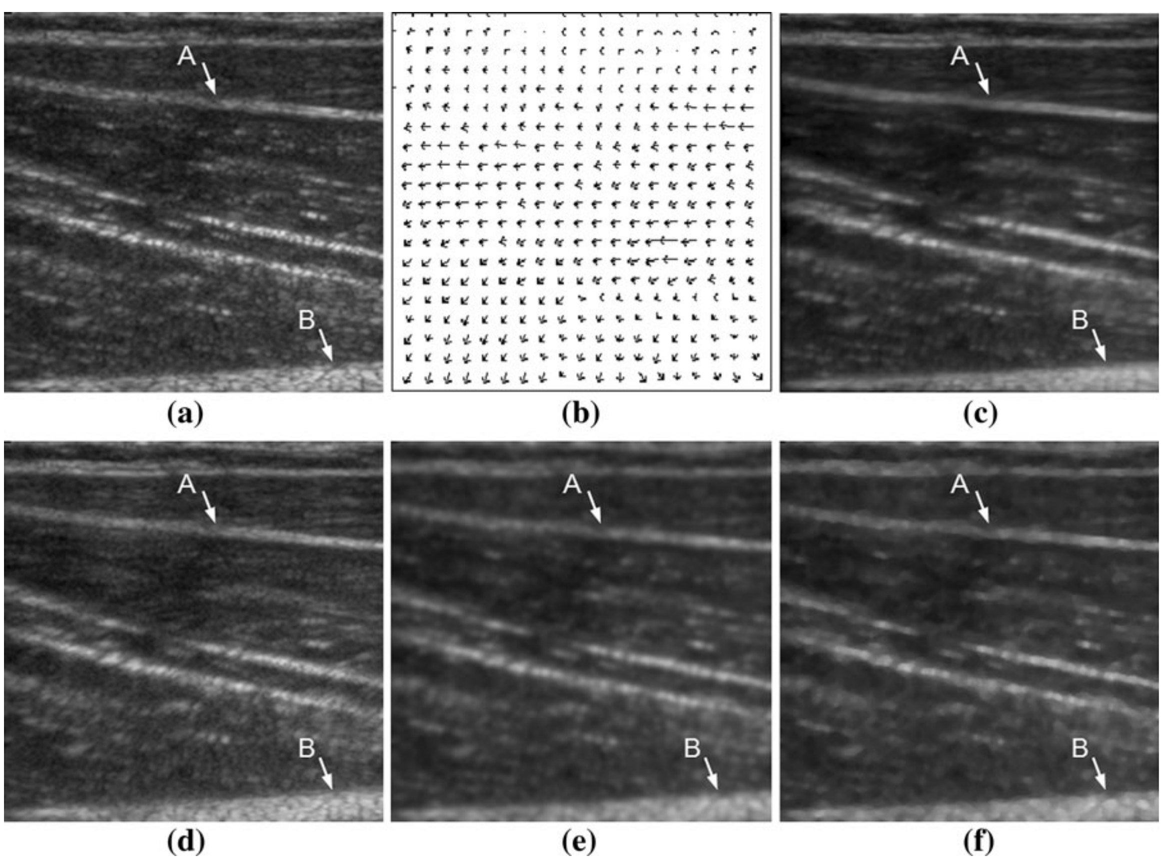

Fig. 5. Example frames of the musculoskeletal experiment: a the original speckle image, b the estimated motion field, c the compound image, d the compound image without motion compensation; e the Gaussian filtered image, f the AWMF filtered image.

Figure 5e,f shows these Gaussian and AWMF filtered images, respectively.

As can be seen in the experimental results, the compound image shows the muscle texture more clearly and preserves more details. The fibrillar appearance of the muscle is more uniformly and continuously displayed, as indicated by arrow A. Also, the compound image shows a continuous and contrast enhanced bone surface boundary, as indicated by arrow B. Generally, the Gaussian and AWMF filtered images are over smoothed, resulting in a loss of some of the fine details and a reduction in spatial image resolution. Image compounding is more helpful in defining the object boundaries in motion image analysis.

In the myocardial experiment, echocardiographic images of the left ventricle (LV) were acquired. Figure 6 shows an example of a short-axis view echocardiography. In this data set, the speckle decorrelations are particularly large due to cardiac contraction. Figure 6a,e shows example frames of the sequence during systolic and diastolic periods, respectively, and Figure 6b,f shows the corresponding estimated motion fields. The typical contraction and expansion of a normal beating heart during systole and diastole are captured and estimated as the motion fields from sonographic image sequences. Although it was not possible to measure the true motion vectors, the estimated motion vector fields could fill the needs of inter-frame correspondence in the compounding computation and achieved good consistency with the observations of the clinician. Figure 6c,g shows the compound images and Figure 6d,h shows the AWMF-filtered images of Figure 6a,e, respectively.

In the myocardial experiment, the given B-scan image sequence generally contains two homogeneous regions: the myocardium and the ventricle part. Therefore, the effect of motion compounding on the image statistics could be investigated by calculating the speckle SNR and CNR. Figure 7a shows an example frame of an echocardiography sequence and Figure 7b shows the compound image. Figure 7c,d shows the Gaussian filtered image with $\sigma=1$ and $\sigma=5$, respectively. Figure 7e shows the AWMF filtered image. Table 1 shows the calculated speckle SNRs and CNRs by using different methods. As shown in Table 1, the speckle SNR and CNR of the Gaussian filtered images increase when the selected σ increases. When $\sigma=5$, the CNR for the Gaussian filtering was close to the compound image. However, the

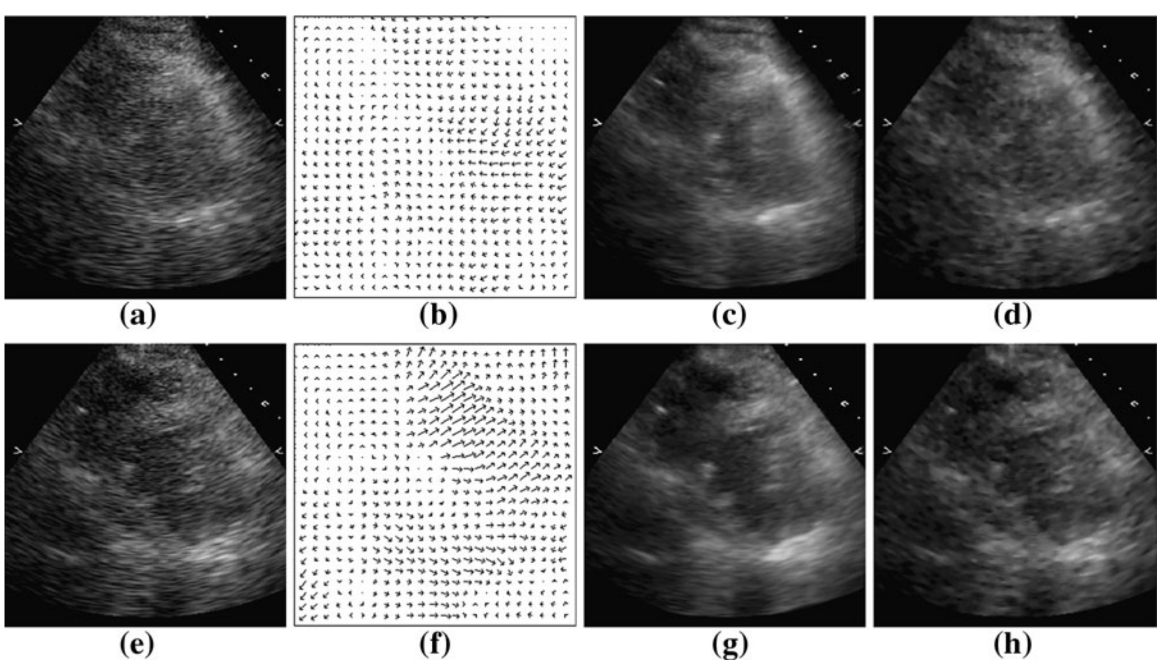

Fig. 6. Example frames of the short-axis view echocardiography experiment during systole (*top row*) and diastole (*bottom row*): a and e the original speckle images, b and f the estimated motion fields, c and g the compound images, d and h the AWMF filtered images.

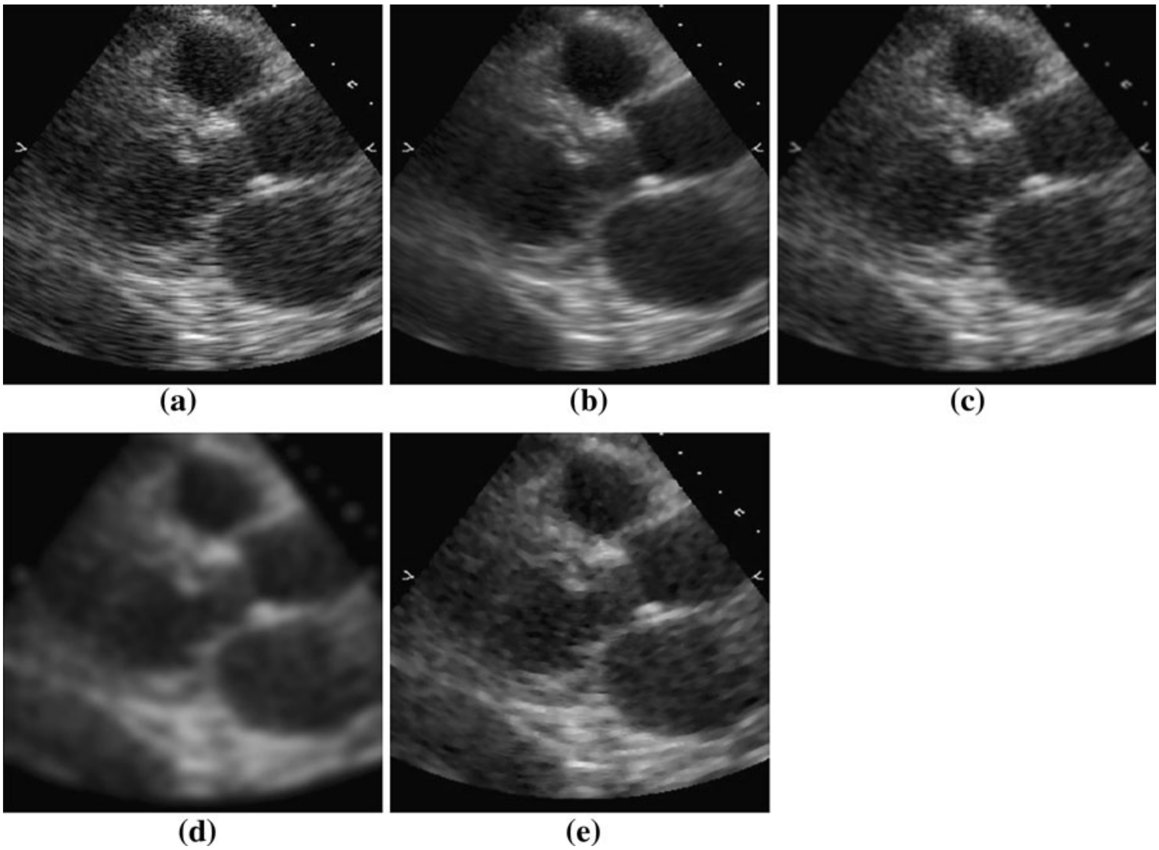

Fig. 7. Example frames of the echocardiography experiment: a the original speckle image, b the compound image, c the Gaussian filtered image (with $\sigma = 1$); d the Gaussian filtered image (with $\sigma = 5$); e the AWMF-filtered image.

Gaussian-filtered images appeared to be significantly over-smoothed and the texture details were smoothed out. According to these results, the proposed motion compounding technique outperformed the spatial filters, with a higher SNR and CNR, while keeping more texture details.

Table 2 shows the calculated speckle SNRs and CNRs of several echocardiography sequences. According to the experimental results, the proposed motion compounding provided a significant improvement in both speckle SNR and CNR compared to other spatial filters. Visual inspection showed that the proposed motion compounding technique also improved image quality by reducing speckle noise and increasing ventricular border definition. These improvements also help with further image analysis, such as segmentation and tracking.

More clinical results are available on http://vision.csie.ncku.edu.tw/~linjs/USCompound/.

DISCUSSIONS

In the proposed method, speckle tracking is used to find the in-plane motion resulting from the target movement and images can then be spatially matched before being compounded. Therefore, one

Table 1. The Calculated SNRs and CNRs by Using Different Methods

	$SNR_{myo.}$	$SNR_{vent.}$	CNR
Speckle image	2.31	1.42	4.71
Compound image	2.69	3.31	10.27
Gaussian filtered image ($\sigma = 1$)	2.54	1.76	5.98
Gaussian filtered image ($\sigma = 2$)	2.77	2.20	7.43
Gaussian Filtered Image ($\sigma = 3$)	2.99	2.57	8.64
Gaussian filtered image ($\sigma = 4$)	3.21	2.89	9.63
Gaussian filtered image ($\sigma = 5$)	3.45	3.18	10.44
AWMF image	2.63	1.77	6.24

Table 2. The Calculated SNRs and CNRs by Using Different Methods

Echocardiography sequences		6203	6204	6205	6206
	SNR_{myo}	2.54	2.72	2.48	3.33
	$SNR_{vent.}$	0.90	1.01	0.91	1.02
Speckle image	CNR	6.86	6.17	5.92	7.03
	SNR_{myo}	3.27	3.39	3.49	4.52
	$SNR_{vent.}$	2.38	2.65	2.86	3.52
Compound image	CNR	12.68	12.29	12.33	16.65
	SNR_{myo}	2.75	3.00	2.79	3.77
	$SNR_{vent.}$	1.10	1.35	1.27	1.35
Gaussian filtered image ($\sigma = 1$)	CNR	8.73	8.56	8.79	9.79
	SNR_{myo}	2.86	3.11	2.80	3.96
	$SNR_{vent.}$	0.99	1.21	1.16	1.28
AWMF image	CNR	8.87	8.50	9.59	10.39

potential problem of the proposed motion compounding is the out-of-plane problem. When it occurs, the observed object moves out of the imaging plane during image acquisition. Thus, pixels might not be correctly registered for compounding and artifacts might be generated. Therefore, in the experiments, the probe was placed as parallel to the moving direction of the observed muscle as possible to minimize the out-of-plane problem.

On the other hand, modifying the compound operator may help to solve the out-of-plane problem. The compounding operator can be modified by using a weighted mean or a weighted median strategy. The weighting criteria can be defined based on local characteristics or temporal distance. Similar local characteristics or shorter temporal distances are assigned higher weighting. In myocardial experiments, a temporal realignment might also be useful because of the periodicity of cardiac motion. That is, image sequences can be scanned with more cardiac cycles and then resorted according to their corresponding time phases. Frames in similar time phases, which correspond to similar physical positions, can then be selected for compounding. To further verify the out-of-plane problem, a 4D compounding technique that is free from the out-of-plane problem can be developed and we are currently working on 4D cases.

CONCLUSION

In this paper, we proposed a new software-based motion compounding system to improve the image quality of ultrasound image sequences. The proposed method does not require a special hardware platform and can be implemented as a standalone software system. The proposed motion compounding concept can successfully average adjacent frames, which are registered and warped to the reference image, to generate a compound image with reduced speckle noise and enhanced contrast. By adopting a hierarchical structure, we apply the adaptive feature weighted technique to estimate the motion field in multiple resolutions. This approach was found very effective in reliable motion tracking for ultrasound images. Thus the compound images can preserve correct texture details and reduce artifacts generated by speckle noises and target movement. The experiments also achieve significantly higher SNR and CNR values that reflect the improvements in speckle reduction and contrast enhancement. Generally the proposed compounding method is valuable in improving the quality of regularly acquired ultrasound images for better visualization, clinical assessment, and image postprocessing.

ACKNOWLEDGEMENTS

The authors wish to express their appreciation for the support from the National Science Council under contract NSC91-2213-E-006-060. Also, this work made use of shared facilities supported by the Program of Top 100 Universities Advancement, Ministry of Education, Taiwan, R.O.C. The authors also like to thank Professor Pai-Chi Li, National Taiwan University, for providing phantom images and helpful discussions.

REFERENCES

1. Healey AJ, Leeman S: Speckle reduction methods in ultrasound pulse-echo imaging. IEEE Proc. of Acoustic Sensing and Imaging 68–76, 1993

2. Evans AN, Nixon MS: Mode filtering to reduce ultrasound speckle for feature extraction. IEEE Proc Vis Image Signal Process 142(2):87–94, 1995

3. Souquet J: State of the art in digital broadband medical ultrasound imaging. Comptes Rendus de l'Academie des Sciences Series IV Physics 2(8):1091–1098, 2001

4. Entrekin R, Jackson P, Jago JR, Porter BA: Real time spatial compound imaging in breast ultrasound: technology and early clinical experience. Medica mundi 43(3):35–43, 1999

5. Rafiee A, Moradi MH, Farzaneh MR: Novel genetic-neuro-fuzzy filter for speckle reduction from sonography images. J Digit Imaging 17(4):292–300, 2004

6. Rohling R, Gee A, Berman L: Three-dimensional spatial compounding of ultrsound images. Med Image Anal 1(3):177–193, 1997

7. Krücker JF, Meyer CR, LeCarpentier GL, Fowlkes JB: 3D spatial compounding of ultrasound images using image-based nonrigid registration. Ultrasound Med Biol 26(9):1475–1488, 2000

8. Techavipoo U, Chen Q, Varghese T, Zagzebski JA, Madsen EL: Noise reduction using spatial-angular compounding for elastography. IEEE Trans Ultrason Ferroelectr Freq Control 51(5):510–520, 2004

9. Cincotti G, Loi G, Pappalardo M: Frequency decomposition and compounding of ultrasound medical images with wavelet packets. IEEE Trans Med Imag 20(8):176–771, 2001

10. Li P-C, Wu C-L: Strain compounding: spatial resolution and performance on human images. Ultrasound Med Biol 27 (11):1535–1541, 2001

11. Jespersen SK, Wilhjelm JE, Sillesen H: In vitro spatial compound scanning for improved visualization of atherosclerosis. Ultrasound Med Biol 26(8):1357–1362, 2000

12. Entrekin RR, Porter BA, Sillesen HH, Wong AD, Cooperberg PL, Fix CH: Real-time spatial compound imaging: application to breast, vascular, and musculoskeletal ultrasound. Semin Ultrasound, CT, and MRI 22(1):50–64, 2001

13. Kofoed SC, Grønholdt M-LM, Wilhjelm JE: Real-Time spatial compound imaging improves reproducibility in the evaluation of atherosclerotic carotid plaques. Ultrasound Med Biol 27(10):1311–1317, 2001

14. Huber S, Wagner M, Mdel M, Czembirek H: Real-time spatial compound imaging in breast ultrasound. Ultrasound Med Biol 28(2):155–163, 2002

15. Xue K, He P, Wang Y: A motion compensated ultrasound spatial compounding algorithm. Proc. of 19th Intl. Conf. of IEEE EMBS 2:818–, 821, 1997

16. Groves AR, Rohling RN: Two-dimensional spatial compounding with warping. Ultrasound Med Biol 30(7):929–942, 2004

17. Lukin V, Ponomarenko N, Bunaeva I: Post-processing of multi-look and sequentially formed images in radar and ultrasonic coherent systems. Proc. of 46th IEEE Intl. Midwest Symp. on Circuits and Systems 2:745–751, 2004

18. Friemel BH, Bohs LN, Trahey GE: Relative performance of two-dimensional speckle-tracking techniques: normalized correlation, non-normalized correlation and sum-absolute-difference. Proc. of IEEE Ultrasound Symposium 1481–1484, 1995

19. Yeung F, Levinson SF, Parker KJ: Multilevel and motion model-based ultrasonic speckle tracking algorithms. Ultrasound Med Biol 24(3):427–441, 1998

20. Pellot-Barakit C, Frouin F, Insana MF, Herment A: Ultrasound elastography based on multiscale estimations of regularized displacement fields. IEEE Trans Med Imag 23 (2):153–163, 2004

21. Lin CH, Lin MCJ, Sun YN: Ultrasound motion estimation using a hierarchical feature weighting algorithm. Comput Med Imaging Graph 31(3):178–190, 2007

22. Strintzis MG, Kokkinidis I: Maximum likelihood motion estimation in ultrasound image sequences. IEEE Signal Process Lett 4(6):156–157, 1997

23. Bergeron C, Dubois E: Gradient-based algorithms for block-oriented MAP estimation of motion and application to motion-compensated temporal interpolation. IEEE Trans Circuits Syst Video Technol 1(1):72–85, 1991

24. Li W, Salari E: Successive elimination algorithm for motion estimation. IEEE Trans Image Process 4(1):105–107, 1995

25. Lu JY, Wu KS, Lin JC: Fast full search in motion estimation by hierarchical use of Minkowski's inequality (HUMI). Pattern Recogn 31(7):945–952, 1998

26. Chen YS, Hung YP, Fuh CS: Fast block matching algorithm based on the winner-update strategy. IEEE Trans Image Process 10(8):1212–1222, 2001

27. Wagner RF, Smith SW, Sandrik JM: Statistics of speckle in ultrasound B-scans. IEEE Trans Sonics Ultrason SU-30 (3):156–163, 1983

28. Loupas T, McDicken WN, Allan PL: An adaptive weighted median filter for speckle suppression in medical ultrasonic images. IEEE Trans Circuits Syst 36(1):129–135, 1989

29. Karaman M, Kutay MA, Bozdagi G: An adaptive speckle suppression filter for medical ultrasonic imaging. IEEE Trans Med Imaging 14(2):283–292, 1995

30. Sikora T: Trends and perspectives in image and video coding. Proc IEEE 9(1):6–17, 2005

31. Kotropoulos C, Magnisalis X, Pitas I, Strintzis MG: Nonlinear ultrasonic image processing based on signal-adaptive filters and self-organizing neural networks. IEEE Trans Image Process 3(1):65–77, 1994

32. Wilhjelm JE, Jensen MS, Brandt T, Sahl B, Martinsen K, Jespersen SK, Falk E: Some imaging strategies in multi-angle spatial compounding. Proc. of 2000 IEEE Ultrasonics Symp. 1615–1618, 2000

33. Xu C, Prince JL: Snakes, shapes, and gradient vector flow. IEEE Trans Image Process 7(3):359–369, 1998